

Flow induced coating of fluoropolymer additives: Development of frustrated total internal reflection imaging

S. B. Kharchenko, P. M. McGuiggan, and K. B. Migler^{a)}

*Polymers Division, National Institute of Standards and Technology, Gaithersburg,
Maryland 20899-8544*

(Received 19 May 2003; final revision received 25 July 2003)

Synopsis

In the extrusion of linear low-density polyethylene (PE), fluoropolymer processing additives (PPAs) are used to eliminate the surface defect known as “sharkskin” by coating the die wall and inducing slip at the PPA/PE interface. We describe an *in situ* optical method for measurement of the coating thickness by exploiting the phenomenon of frustrated total internal reflection. By correlating the optical and pressure measurements, extrudate appearance and auxiliary experiments, we can elucidate the kinetics of the coating process. The PPA droplets first adsorb in the entrance region of the die and migrate under shear stress towards the capillary exit where they act to suppress sharkskin. We find that a uniform coating in the range of 25–60 nm is sufficient for sharkskin elimination. The steady state coating thickness near the exit ranges from 200 to 400 nm depending on the shear rate and concentration. We develop a mass balance model for calculation of the steady state coating thickness which compares well with our experimental data. © 2003 The Society of Rheology. [DOI: 10.1122/1.1619375]

I. INTRODUCTION

Flow instabilities in polymer processing operations such as extrusion, injection molding, wire coating, film casting and blowing have a significant negative impact on product appearance and performance. Elimination of the instabilities without sacrificing product quality is possible if the inherent relationships between polymer molecular dynamics and flow boundary conditions are well understood. This stimulates research to explore novel materials and methods.

In the present work, we focus on the extrusion of linear low-density polyethylene through cylindrical and slit dies driven by an imposed volumetric flow rate. When the corresponding stress level is sufficiently low (below approximately 0.1 MPa [Hatzikiriakos *et al.* (1995); Inn *et al.* (2000)]), the extrudate appearance is smooth. In general, for increased levels of stress, the polymer flow becomes unstable, leading to various types of melt fracture. First, the extrudate surface becomes distorted, and shows discrete ridges whose amplitude and wavelength increase with the wall shear stress [Mackley *et al.* (1998); Inn *et al.* (2000)]. This flow instability problem is known as sharkskin [Howells and Benbow (1962)], and has been recently reviewed by Larson (1992), Graham (1999) and Denn (2001). Sharkskin can be the rate limiting factor in manufacturing because it occurs at lower extrusion rates than other instabilities, such as spurt flow and gross melt

^{a)}Author to whom correspondence should be addressed; electronic mail: kalman.migler@nist.gov

fracture (GMF). During spurt flow, the polymer surface exiting the die appears to be a combination of partially ruptured (similar to sharkskin) and glossy regions [Vinogradov (1975)]. GMF occurs at even higher stress when unstable vortices form at the entry region of the die, and the flow becomes highly asymmetric, producing large scale distortion of the extrudate [Petrie and Denn (1976); Kalika and Denn (1987); Piau *et al.* (1988, 1990); Kim and Dealy (2002a, 2002b)]. The present paper confines itself to the sharkskin problem because this is where the fluoropolymer additives are found to be the most effective.

The precise origin of sharkskin is still unresolved, but it is known that the flow boundary condition in the vicinity of the die exit strongly influences its occurrence. Through visualization studies using colorized materials [Bergem (1976)], flow birefringence measurements [El Kissi and Piau (1994); Piau and Agassant (1996); Mackley *et al.* (1998); Barone and Wang (2001)], depth-resolved optical microscopy [Migler *et al.* (2001b)], and by locally precoating a die [Moynihan *et al.* (1990); Wang *et al.* (1996); Dhori *et al.* (1997)], it has been generally agreed that the site of initiation of sharkskin is the die exit. A region of high stress has been identified in this area that points to the existence of a analytical singularity. A widely held picture is that as polymer melt leaves the die, the layer adjacent to the wall at the exit (which flows with the slowest velocity) must suddenly accelerate, and impose strong stretching of the polymer chains. The polymer ruptures at the free surface when stress levels exceed a critical tensile stress [Cogswell (1977); Inn *et al.* (1998)]. This idea was further elaborated upon using high-speed video microscopy and it was concluded that the *reconfiguration rate* was a critical parameter that defines the onset of sharkskin regardless of the stick or slip boundary condition [Migler *et al.* (2002)].

One method to suppress sharkskin is to modify the boundary condition at the polymer/wall interface. Different surface energy dies such as gold, copper, brass, aluminum, glass and Teflon were effectively correlated with the onset of instability [Ramamurthy (1986); Hatzikiriakos *et al.* (1995); Piau and Agassant (1996); Person and Denn (1997); Ghanta *et al.* (1999)]. For example, for the Teflon-coated and brass dies in those studies, smooth extrudates were obtained at higher flow rates than for steel dies. However, in the industrial environment, these slippery surfaces are unsuitable because they are too soft and will degrade or scratch over time.

A widely used industrial method to modify the boundary is to add a small amount of a fluoropolymer (also referred to as fluoroelastomer) processing additive (PPA) into the mainstream polymer, thereby creating an immiscible blend. A recent overview of various processing aids, their formulations, applications and performance was given by Amos *et al.* (2001) and by Achilleos *et al.* (2002). The general view of the coating process of an extruder that initially contains pure polyethylene (PE) is that the immiscible PPA droplets somehow migrate toward the die wall during extrusion and form a coating layer. The PE then slips at the PPA/PE interface [Shih (1976); Kanu and Shaw (1982); Hatzikiriakos and Dealy (1993)], and for a fixed volumetric flow rate this results in a decrease of extrusion pressure and wall shear rate. After a period of induction, during which the pressure continues to decrease, the sharkskin is gradually eliminated. The elimination is not homogeneous, but rather one observes "clear streaks" in the extrudate which increase in number and width, until the entire extrudate surface is sharkskin free. It is known that in order for the fluoropolymer to be effective, it must be present at the die exit [Moynihan *et al.* (1990); Wang *et al.* (1996); Dhori *et al.* (1997); Migler *et al.* (2002)], where the slippage of the PE alleviates the stress singularity and dramatically weakens the deformation rate of the polymer [Rosenbaum *et al.* (1995)].

Thus the PPA/PE system is an important motivator for the study of polymer–polymer slippage, which was first reported by a rheological experiment by Lyngaae-Jorgensen (1998). From the standpoint of microscopic scaling theories [Brochard-Wyart (1990); Brochard-Wyart *et al.* (1992); Brochard-Wyart and de Gennes (1993); Goveas and Fredrickson (1998)], local heterogeneity between the PPA and the mainstream polymer chains leads to the reduction in entanglement density (and therefore, viscosity) at their interface, leading to effective slippage. The first direct measurements of polymer–polymer slippage were made optically by Migler *et al.* (2001b, 2002) and also by Lam *et al.* (2003). Measurements of polymer–polymer slippage on coextruded multilayers were made by Zhao and Macosko (2002) who also showed that it was suppressed by a compatibilizer. The role of polymer–polymer slip was discussed by Park *et al.* (2003) in the case of droplet coalescence.

The kinetics of the coating of the exit of the internal die wall by the PPA is critical to its effectiveness, yet it is perhaps the least understood aspect of PPA behavior. In fact, the major metric used to evaluate the efficacy of a given PPA is the time it takes to completely eliminate sharkskin. However, there is no fundamental understanding of this coating process. In Poiseuille type of flow through a cylindrical die the direction of motion of suspended deformable droplets may be controlled by the rate of shear and droplet viscoelasticity. Through direct experimental measurements [Oliver (1962); Shizgal *et al.* (1965)] as well as via numerical simulations [Chan and Leal (1979); Zhou and Pozrikidis (1994); Coulliette and Pozrikidis (1998); Li and Pozrikidis (2000); Mortazavi and Tryggvason (2000)] it was found that depending on relative viscosity of the droplets and the suspending media, as well as on the Reynolds number, the droplets which were initially closer to the walls could migrate toward the die axis, and the droplets entering the die at its center, could migrate toward the die wall. However particle-free zones near the walls were identified for all cases. This is in contrast to recent work of Hong *et al.* (1999, 2000) who used x-ray photoelectron spectroscopy and transmission electron microscope techniques and showed that in coextrusion of immiscible hyperbranched polyethylene/linear polyethylene blends, the lower viscosity hyperbranched polyethylene droplets migrated toward the regions of high shear (the wall). It is also known that in Poiseuille flow of bicomponent polymer melts with significantly different viscosities, the equilibrium interface configuration is stated to be controlled by the minimum viscous dissipation, so the higher viscosity compound appears to be encapsulated by the lower viscosity one [Everage (1973); Joseph *et al.* (1984)].

The knowledge gained thus far mainly addresses the phenomenological role of PPA in extrusion of polyolefins under conditions of steady state flow, yet information about the rate at which the PPA coats the die wall, as well as characteristics of the coating, are scarce [Kanu and Shaw (1982); Migler *et al.* (2001a, 2001b); Achilleos *et al.* (2002)]. For example, it was shown that an increase in the concentration of the PPA, its dispersion quality and higher flow rates reduces coating times [Xing and Schreiber (1996); Amos *et al.* (2001); Achilleos *et al.* (2002); Lavallée and Woods (2000)]. In a recent *in situ* microscopy study [Migler *et al.* (2001b)] in which the PE/PPA blend was extruded into a capillary that previously contained only PE, it was observed that the PPA formed streaks in the direction of flow and that the appearance of the streaks coincided with the elimination of sharkskin. However, this technique gives no information about the thickness of the coating and, in particular, no information about the critical thickness for elimination of sharkskin.

In this work, we develop a new measurement technique based on frustrated total internal reflection (frust-TIR) to carry out *in situ* measurements of the coating dynamics and thickness. We address fundamental issues of the coating process such as the thickness

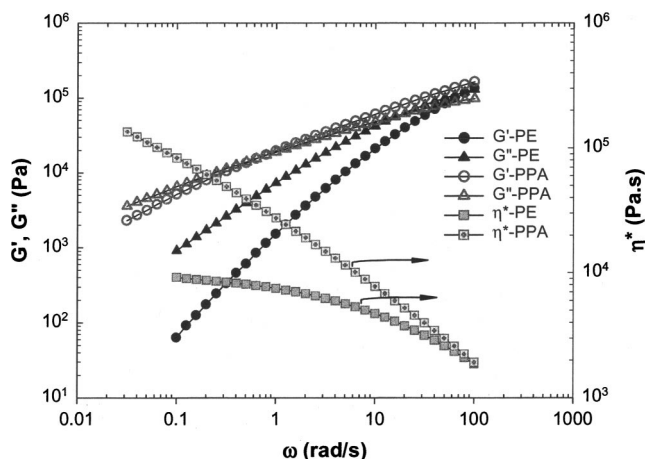


FIG. 1. Viscoelasticity of PE and PPA at $T = 180\text{ }^{\circ}\text{C}$.

necessary to eliminate sharkskin, its steady state value and the location where the PPA droplets leave the melt and coat the wall.

II. EXPERIMENT

A. Materials

Experiments were carried out using ExxonMobil™ linear low-density polyethylene (LLDPE 1001.09 or “PE”) with $\rho = 918\text{ kg/m}^3$, approximate weight-average molecular weight M_w of about 80 kg/mole and melt flow index of 1.0. It contains low levels of an antioxidant and a stabilizer, and some short-chain branching (ethylene butene), which is known to have a negligible effect on polymer viscoelasticity [Wood-Adams *et al.* (2000)]. Additionally, when tested rheologically, it was found that the Cox–Merz rule [Ferry (1980)] was obeyed well. During extrusion, PE readily shows sharkskin melt fracture at a temperature of 180 °C and apparent shear rates $\dot{\gamma} \geq 35\text{ s}^{-1}$. The polymer is transparent in the visible range of wavelengths, with an estimated refractive index (n) of 1.471 ± 0.002 at $\lambda = 633\text{ nm}$ (unless otherwise noted, the \pm represents uncertainties of the measured values and refers to one standard deviation of the observed value).

The fluoroelastomer PPA used in this work was Viton® FreeFlow™ (commercially known as A-500 or FE-X), and it was donated by DuPont Dow Elastomers. This PPA is a copolymer of vinylidene fluoride and hexafluoropropylene (in a 3/2 mass ratio), with an estimated n of 1.371 ± 0.002 . It is nearly twice as dense as PE ($\rho = 1800\text{ kg/m}^3$), has weight-average molecular weight M_w of about 170 kg/mole and a polydispersity index of 3.5. The viscosity at the lowest shear frequency measured in advanced rheometric expansion system (ARES) at $T = 180\text{ }^{\circ}\text{C}$, using 25 mm parallel disk geometry, exceeds that of PE by more than a factor of 10 (Fig. 1). However, at shear frequency of 112.5 s^{-1} both PE and PPA possess comparable viscosity numbers, i.e., PPA has a higher degree of shear thinning.

Critical factors defining the PPA/PE blend morphology are the viscosity ratio, composition, elasticity, shear stress, interfacial tension and size effects. Starting with mass fraction of 5% (master batch obtained from DuPont Dow Elastomers with controlled droplet size distribution), 0.1% and 0.5% PPA/PE blends were prepared using a HAAKE twin-screw extruder [Migler *et al.* (2002)] operating at 1.36 rad/s and barrel section

temperatures of 160, 180 and 190 °C. As a result, PPA droplets of weight-average diameter of $\approx 2 \mu\text{m}$ were obtained. Characterization of the PPA size distribution in the PE matrix was done by collecting a series of microscope images using a 100 \times objective lens.

B. Apparatus for frust-TIR and measurement procedure

Frust-TIR is ideally suited to the *in situ* measurement of coating kinetics and thickness. Before describing it, we first review TIR and its application to rheology. The well known phenomenon of total internal reflection occurs when light that is initially in a material of higher refractive index impinges on a material of lower refractive index at an angle that exceeds a critical value. It was first described by Newton (1730) and the effect appealed to a number of leading scientists such as Fresnel, Stokes, and Quincke because of the existence of energy beyond the boundary [Hall (1902)]. In 1909, the concept that the boundary electric field (called the evanescent wave) in the low index material exponentially decays as a function of distance from the interface was finally formulated [Eichenwald (1909)].

Rheological applications of TIR have appeared in several forms. If the low index material is fluorescent, the evanescent wave can induce fluorescence over a distance that scales as $\lambda/2\pi$, where λ is the wavelength of excitation light [Migler *et al.* (1993)]. These techniques were used to observe the existence of strong slip occurring within a few radii of gyration from the wall. TIR fluorescence spectroscopy was also shown to be a good quantitative tool for describing the kinetics of polymer adsorption and desorption under highly nonequilibrium conditions [Parsons *et al.* (1992)]. In another work [Dao and Archer (2001)], a method of evanescent wave laser polarimetry was developed to investigate near-surface relaxation dynamics of polybutadiene and polystyrene/diethyl phthalate solutions in which the authors were able to demonstrate that the two polymers had different relaxation mechanisms in proximity (80 nm) to the rigid boundary. By applying TIR in microscopy, it was possible to measure the diffusion coefficient of polystyrene microspheres and minute colloidal interactions on the order of 10^{-2} pN [Prieve (1999)]. Interesting findings were reported by Wise *et al.* (1998) who used attenuated total reflectance (ATR) Fourier transform infrared spectroscopy (ATR/FTIR) and evaluated near-wall diffusivity of unentangled and entangled polybutadiene melts. The ATR/FTIR technique was further implemented to explore the effect of the wall on polymer slippage and chain mobility [Wise *et al.* (2000)]. The authors summarized that at the stress levels characteristic of sharkskin, the chain friction coefficient was significantly reduced at a distance several radii of gyration from the wall, leading to apparent slip, whereas under conditions of strong slip, the failure was still adhesive. Another group [Kok *et al.* (2002)] applied ATR/FTIR methodology in pressure driven flows of aqueous suspensions to obtain a direct measure of the polymer droplet concentration in a thin layer near the wall.

In our study, we utilize a different phenomenon known as *frustrated* total internal reflection. Whereas TIR is used at the interface between two semi-infinite media, frust-TIR is used in the case of three media where the thickness of the middle material is $0(\lambda)$ and its refractive index is lower than that of the other two materials. Fortuitously, these conditions are met in our study when we use sapphire for the wall, PPA for the middle material and PE for the third. If one shines light from the sapphire onto the interface at an angle greater than the critical angle for total internal reflection of the sapphire/PPA, and if the PPA is sufficiently thin, some of the light is transmitted through the “forbidden” PPA region and emerges in the PE, thereby “frustrating” the TIR. This phenomenon is known to be used in various methods of measurement of the thickness, refractive index of thin films and absorption versus wavelength spectra [Harrick (1967); McCrackin *et al.*

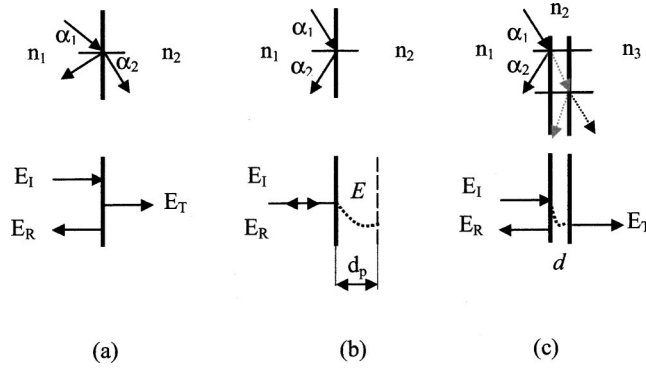


FIG. 2. Refraction and reflection at the smooth boundaries separating (a) two media with $n_1 > n_2$ and $\alpha_1 < \alpha_{\text{crit}}$; (b) two media with $n_1 > n_2$ and $\alpha_1 > \alpha_{\text{crit}}$ (case of TIR); (c) three media with $n_1 > n_2 < n_3$ and $\alpha_1 > \alpha_{\text{crit}}$ (case of frust-TIR). Electric field amplitudes for incident (E_I), transmitted (E_T) and reflected (E_R) waves are shown for each case as well as that of the evanescent field (E).

(2001)]. The direct, nondestructive and noninvasive nature of this technique allows the acquisition of real-time data under conditions of high temperature, pressure and flow in our study.

When light is incident the interface of two media, it is partially transmitted into the second medium and partially reflected back into the first one, as described by Snell's law [Born and Wolf (1993)] [Fig. 2(a)],

$$\frac{\sin(\alpha_1)}{\sin(\alpha_2)} = \frac{n_2}{n_1}, \quad (1)$$

where n_1 and n_2 are the refractive indices of materials at an interface (sapphire/PE or sapphire/PPA), and α_1 and α_2 are incident and refracted angles. A schematic of the electric field amplitudes of incident, transmitted and reflected waves (E_I , E_T , E_R , respectively) is also shown in Fig. 2. When the incident angle is such that α_2 reaches 90° , the condition for TIR is met and the critical angle can be evaluated as $\alpha_c = \sin^{-1}(n_2/n_1)$ [Fig. 2(b)]. Although no light propagates into the second medium there is an exponentially decaying electric field and it is known as the evanescent field [de Fornel (2001)], described by

$$E = E_0 \exp(-Z/d_p), \quad (2)$$

where Z is the distance from the boundary and parameter d_p is defined as the penetration depth:

$$d_p = \frac{\lambda}{2\pi\sqrt{n_1^2 \sin^2 \alpha_1 - n_2^2}}. \quad (3)$$

For example, if n_1 and n_2 in Fig. 2 are equal to 1.766 (sapphire) and 1.371 (fluoropolymer), respectively, then for a He-Ne laser ($\lambda = 633$ nm) and an arbitrary incident angle of 54° [but greater than the critical angle α_c (sapphire/PPA) = 50.93°], the corresponding penetration depth will be 250 nm [Fig. 2(b)].

As mentioned above, frustrated TIR refers to the case where there are three dielectric media (sapphire/PPA/PE, or $n_1/n_2/n_3$) and the middle one (of thickness d) has the lowest refractive index [Fig. 2(c)]. There will then be a range of angles of α_1 such that

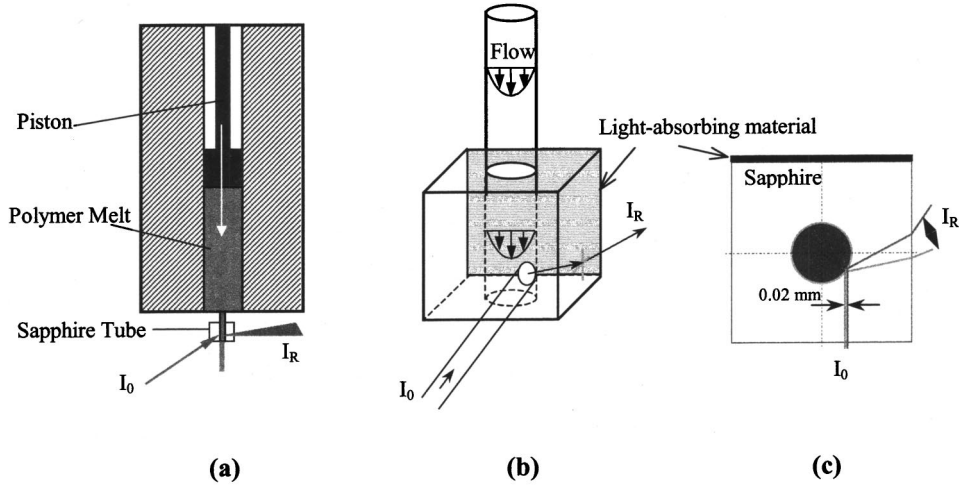


FIG. 3. Rheo-optical apparatus for the FTIR measurements: (a) Capillary rheometer/sapphire die assembly; (b) sapphire die (side view); (c) sapphire die (bottom view). The double arrow shows the range of incident angles of interest. I_0 and I_R are the intensities of incident and reflected light, respectively.

the condition of total internal reflection is met for the (n_1/n_2) interface, but is not met for the (n_1/n_3) interface: $\alpha_c(\text{sapphire/PPA}) = \sin^{-1}(n_2/n_1) < \alpha_1 < \alpha_c(\text{sapphire/PE}) = \sin^{-1}(n_3/n_1)$.

Under these conditions a portion of the incident electric field will be transmitted into the third medium [Fig. 2(c)], and the thickness d of the thin film can be found, described by Court and von Willisen (1964) as

$$d = d_p \operatorname{arcsinh} \left[\frac{1}{\xi_p} \left(\frac{1}{1-R_p} - \beta_p \right) \right]^{0.5}, \quad (4)$$

where R_p is the experimentally measured reflectivity and ξ_p and β_p are defined as

$$\xi_p = \frac{\xi_s}{n} [(N^2+1)\sin^2 \alpha_1 - 1] \times [(n^2 N^2 + 1)\sin^2 \alpha_1 - n^2], \quad (5)$$

$$\beta_p = [(n^2 - \sin^2 \alpha_1)^{0.5} + n^2 \cos \alpha_1]^2 / [4n^2 \cos \alpha_1 (n^2 - \sin^2 \alpha_1)^{0.5}], \quad (6)$$

where $n = n_3/n_1$, $N = n_1/n_2$ and

$$\xi_s = (N^2 - 1)(n^2 N^2 - 1) / [4N^2 \cos \alpha_1 (N^2 \sin^2 \alpha_1 - 1)(n^2 - \sin^2 \alpha_1)^{0.5}]. \quad (7)$$

The frust-TIR is implemented in a capillary rheometer (Goettfert Rheo-Tester 2000) with the 12 mm barrel diameter [Fig. 3(a)]. We extrude through a custommade cylindrical sapphire die ($l/D = 38.2 \text{ mm}/1.6 \text{ mm}$), which replaces a conventional steel or tungsten-carbide one [Figs. 3(b) and 3(c)]. The die is attached to the barrel via a special metal fitting and a Conax die holder. The choice of cylindrical die geometry was made with the intention to have a simple flow setup, although it increases the complexity of the optics compared to flow between parallel plates. A p -polarized wave is generated by a He-Ne laser and a polarizer with the fast axis oriented parallel to the plane of incidence and orthogonal to the sapphire c axis. For this polarization losses due to reflections at interfaces along the optical path are the lowest [Born and Wolf (1993)]. The light impinges on the sapphire die $2 \pm 0.1 \text{ mm}$ upstream of the die exit and its intensity is measured with a

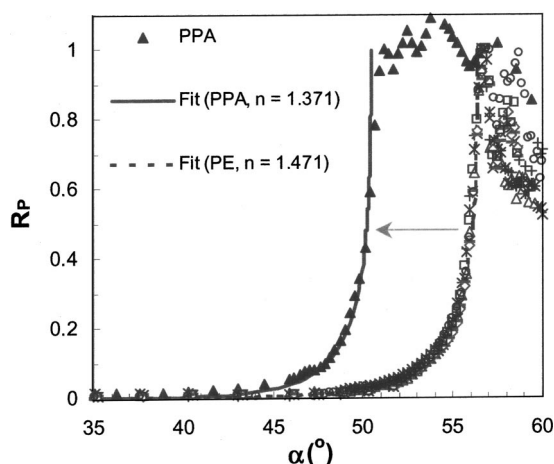


FIG. 4. Reflectivity plots as a function of the angle for two cases where the die is filled with pure PE or pure PPA. The anticipated transition (shown by the arrow) from the reflectivity of the PE to that of the PPA during extrusion of a PPA/PE blend is shown. All symbols other than the closed triangles represent our several experimental reflectivity measurements of the PE.

photodetector mounted on a rotary platform (angular resolution of 0.05°) whose axis of rotation coincides with that of the flow tube.

With our geometry, we measure critical angles for PE (50.93°) and PPA (56.42°) using pure materials, i.e., on the sapphire/PE and sapphire/PPA interfaces. Therefore, to characterize the angular dependency of the reflectivity of *p*-polarized light, the Fresnel relation $R_p = \tan^2(\alpha_2 - \alpha_1) / \tan^2(\alpha_2 + \alpha_1)$ is employed [Born and Wolf (1993)] to fit the experimental data (Fig. 4). The range of angles between 50.93° and 56.42° defines the window of “operational angles” as described by Eq. (1), and it corresponds to a distance of $76.6 \mu\text{m}$ around the die circumference. Because the laser beam has a finite diameter and because it hits the tube perpendicular to the flow axis, light is reflected over a range of angles that cover the operational window. Note that each angle corresponds to a different position on the tube in the circumferential direction [Fig. 3(c)]. In practice we use a narrower range of angles because the sensitivity of the technique is low in the proximity of these two critical angles. Thus, the working range covers a distance of about $63.3 \mu\text{m}$ around the die circumference (or 1.26% of the total die circumference), and the width of light in the flow direction is defined by the beam diameter of approximately 1 mm. Intuitively, as the PPA/PE blend is extruded, a transition from the reflection curve associated with sapphire/PE to that of sapphire/PPA should be observed (Fig. 4). When there is no PPA coating, light incident at an angle of less than 50.93° will be partially transmitted through the die where it can cause spurious reflections. To reduce this, we attached a strongly absorbing (black) material to the back wall of the sapphire die as shown in Figs. 3(b) and 3(c). The Gaussian nature of the intensity of the incident light does not have a strong effect on our measurements because the width of the beam is much larger than our circumferential length defined by operational angles.

In our use of Eq. (4) to analyze the data and extract the fluoropolymer thickness, we utilize the assumption that the fluoropolymer forms a single layer between the wall and the polyethylene. If the interface were diffuse (for example, if there were an intermediate region of droplets of fluoropolymer in PE), our technique would report an effective layer thickness.

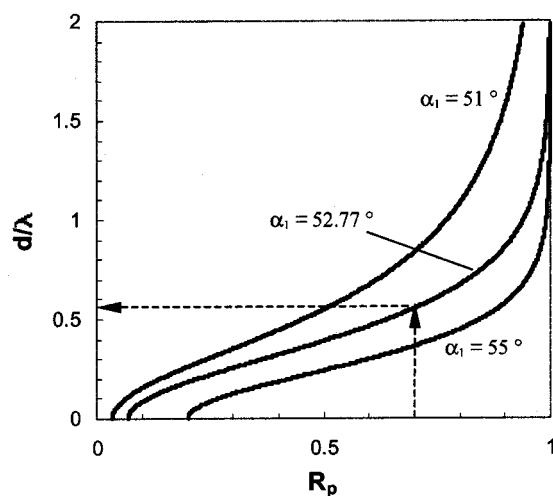


FIG. 5. Evaluation of the coating thickness at a given angle of incidence.

When compared to the spectroscopic techniques discussed above, frust-TIR is inferior in terms of chemical specificity, orientation of particular groups and the need for the middle material to have the lowest refractive index. But it has several advantages, such as quantitative thickness (or refractive index) determination, ability to probe closer to the wall (as low as 20 nm), relative simplicity of operation, inexpensive hardware, and a significantly smaller beam spot size. Another important asset is that the technique is compatible with commercial rheometers as discussed below.

Measurement of the PPA coating kinetics is performed as follows. First, we acquire the reflectivity signals of pure PE during extrusion and at “no flow” conditions, e.g., when the polymer has completely relaxed. This is repeated several times to establish the background reference signal and to estimate the sensitivity of the measurement (Fig. 4). Experiments are conducted at a temperature of 180 °C and at apparent shear rates of 112.5 or 215 s⁻¹ at which PE readily exhibits sharkskin melt fracture. Next, extrusion is continued with either the 0.1% or 0.5% PPA/PE blend run under identical conditions. To obtain a coherent picture of the coating kinetics, three signals are correlated: the pressure, the reflectivity and the extrudate surface appearance.

The coating thickness may be estimated at a given incident angle ($\alpha_1 = 52.77^\circ$ was arbitrarily chosen) by experimentally obtained R_p and using Eq. (4) (Fig. 5). Also, we can obtain the coating thickness as a function of the circumferential position by sweeping the detector, as long as α_1 is within the operational window described above. This gives us information about the uniformity of the coating over small length scales. In practice, the capillary rheometer works in batch mode and the detector sweeps are carried out during the reloading process. The advantage of determining the thickness during the quiescent reloading time is that we do not have to worry about effects of shear induced temperature excursions, flow birefringence or pressure induced changes in birefringence. Complete polymer relaxation and the absence of the above-mentioned effects are verified by performing reflectivity sweeps using both p and s waves. Information on the coating thickness is reported only when the critical angles for the TIR estimated with each polarization coincide.

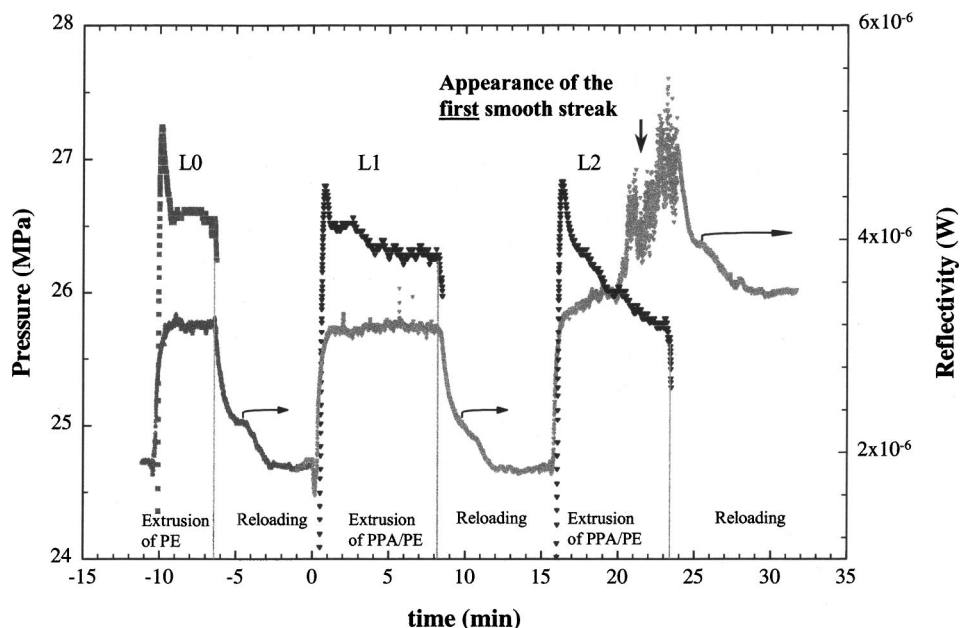


FIG. 6. Effect of the development of the PPA coating during the extrusion of 0.1% PPA/PE blend ($L1-L5$) on the (a) pressure and (b) reflectivity measured at $\dot{\gamma} = 112.5 \text{ s}^{-1}$, $T = 180^\circ\text{C}$ and $\alpha_1 = 52.77^\circ$.

III. RESULTS AND DISCUSSION

Figures 6 and 7 capture the extrusion of pure PE followed by 0.1% PPA/PE and 0.5% PPA/PE blends, respectively, both run at an apparent shear rate of $\dot{\gamma} = 112.5 \text{ s}^{-1}$. The switch from pure PE to the PE/PPA blend occurs at $t = 0 \text{ min}$. The experiments with the 0.5% PPA/PE blend are continued by extrusion of pure PE, as discussed later [Fig. 8(b)].

Figure 6 shows plots of pressure with simultaneous reflectivity measurements versus experimental running time for the 0.1% PPA/PE blend. The experimental running time comprises the extrusion time plus quiescent time needed for reloading. To describe the data we will operate in terms of the extrusion time and load number e.g., $L0$, $L1$, $L2$ etc. To aid in readability only the first two blend batches are displayed in Fig. 6. In Fig. 7 a total of four 0.5% PPA/PE batches ($L1-L4$) are displayed along with postextrusion optical microscopy images taken with a $2.5\times$ objective lens. To demonstrate that the system reached a steady state, measurements of pressure and reflectivity for the last load ($L8$) are also shown.

For the 0.1% PPA/PE blend (Fig. 6), by the end of the first load ($L1$) the pressure is reduced by 1.3%, however, there is no noticeable change in reflectance (on average, less than 0.5%). During the second load ($L2$), the decrease in the pressure is detected from the beginning of the load and the optical signal starts increasing, and develops strong fluctuations. At 6.1 min into $L2$ the first fracture-free streak is detected. By this time the reflectivity has increased by about 40% compared to that of the pure PE.

A qualitatively similar chronological observation can also be made about the blend having a higher content of fluoropolymer droplets, for which the overall coating process is much faster (Fig. 7). The pressure first starts decreasing 3 min into $L1$, and the increase in reflectivity occurs after 3.8 min. At the end of $L1$, the extrudate contains sharkskin everywhere, however, postextrusion microscopy demonstrates that its amplitude and

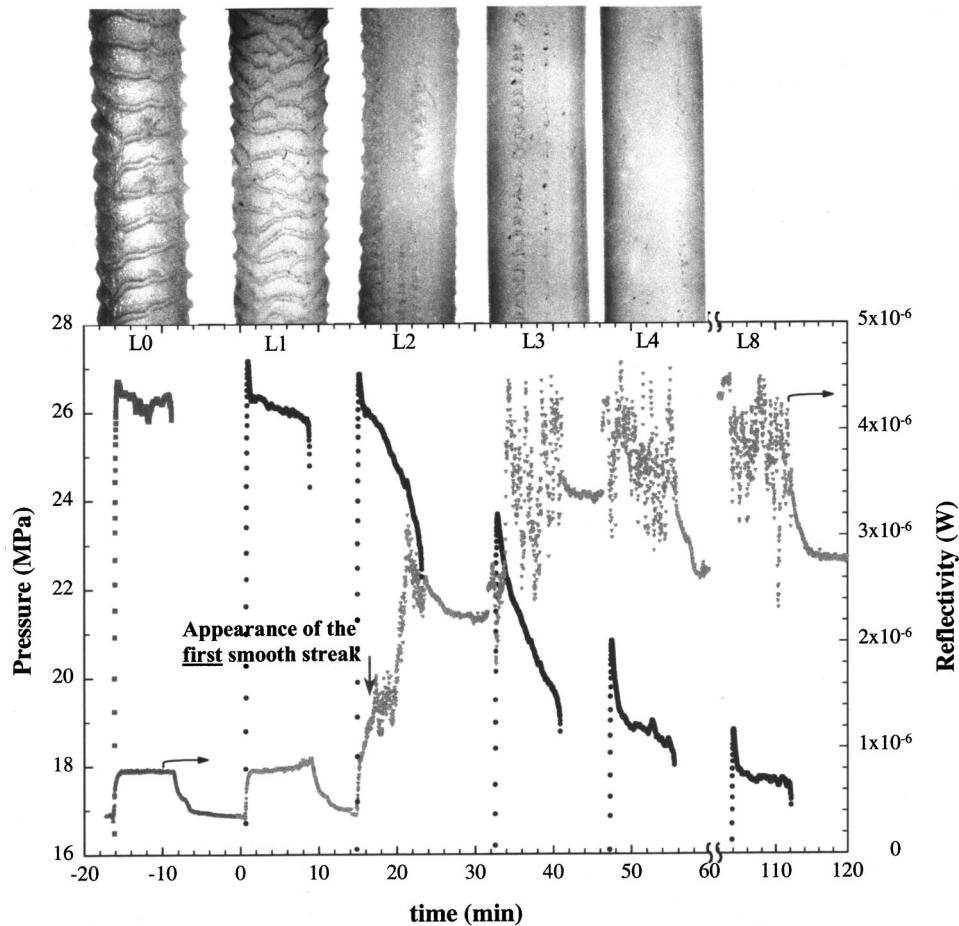


FIG. 7. Effect of the development of the PPA coating during the extrusion of 0.5% PPA/PE blend ($L1-L8$) shown for the four blend loads on the (a) pressure and (b) reflectivity. Measurements were conducted at $\dot{\gamma} = 112.5 \text{ s}^{-1}$, $T = 180 \text{ }^\circ\text{C}$ and $\alpha_1 = 52.77^\circ$.

wavelength have decreased. Such behavior is reminiscent of the sharkskin appearance at essentially lower wall shear stresses [Beaufils *et al.* (1989); Mackley *et al.* (1998); Inn *et al.* (2000)], and may infer the occurrence of partial slippage at the PPA/PE interface or slippage upstream of the exit, which reduces fracture, but does not eliminate it completely. The first sharkskin-free streak is detected 2.3 min into $L2$ when the magnitude of dynamic reflectivity increased by approximately 60% relative to that of the pure PE. Thus, there is a lag of approximately 6 and 2 min (for 0.1% and 0.5% for the PPA/PE blend, respectively) between the first appearance of the fluoropolymer 2 mm upstream of the exit and the appearance of the first sharkskin-free streak. The reasons for this lag are not resolved, but it is likely that the initial coating, being streak like, contains too many bare spots yet provides sufficient slippage. Another is that the fluoropolymer is sufficiently thin at its leading lip that it takes a long time to migrate the last 2 mm.

The uncertainty in our minimum coating thickness measurement was estimated by extruding several (eight) loads of pure PE and collecting the angular reflectivity signals (Fig. 4). Using Eq. (4), the sensitivity of the measurement appears to be $\pm 10 \text{ nm}$. As was described in Sec. II, we capture the evolution of the coating by performing angular

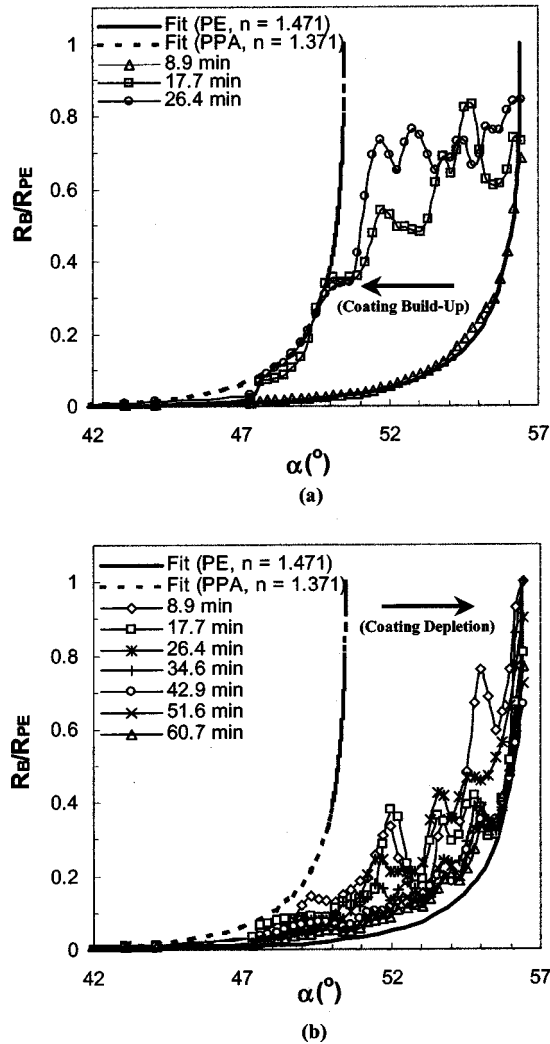


FIG. 8. Angular dependence of the reflectivity during (a) coating build-up (extrusion of the 0.5% PPA/PE blend) followed by (b) coating depletion (extrusion of the pure PE). Measurements were conducted at $\dot{\gamma} = 112.5 \text{ s}^{-1}$ and $T = 180^\circ\text{C}$.

reflectivity sweeps after each extrusion load of the blend. Figure 8(a) shows this for the three first loads (at $t = 8.9$, 17.7 and 26.4 min) of the 0.5% PPA/PE blend at $\dot{\gamma} = 112.5 \text{ s}^{-1}$. The actual coating thickness d is plotted as a function of time versus the circumferential length of the die wall in Fig. 9. Note that since our angular reflectivity measurements cover about 1.26% of the total die circumference, it may limit optical determination of the appearance of the initial streaks.

From Fig. 8(a) it can be seen that after $L1$ of the 0.5% PPA/PE blend ($t = 8.9$ min, Fig. 7), the optical signal in the operational window of incident angles is only marginally greater than that of the PE. Therefore, the estimate of $d = 25 \pm 10 \text{ nm}$ [Fig. 9(a)] is on the order of standard uncertainty of the measurement, even though, as seen from Fig. 7, the reflectivity signal observed at the single angle of incidence $\alpha_1 = 52.77^\circ$ during extrusion clearly increases, hinting at the presence of PPA at the wall. As extrusion continues,

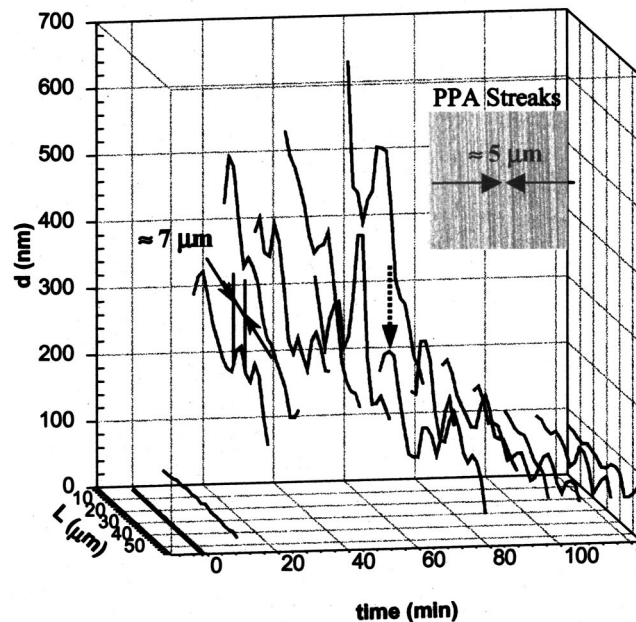


FIG. 9. Visualization of the PPA coating kinetics during extrusion of the (a) 0.5% PPA/PE blend followed by extrusion of the pure PE (shown by the dashed arrow) at $\dot{\gamma} = 112.5 \text{ s}^{-1}$ and $T = 180 \text{ }^\circ\text{C}$.

the reflectivity signal exhibits pronounced local maxima and minima, as seen at the end of the second load ($t = 17.7 \text{ min}$) [Fig. 8(a)]. At that time the signal has reached two maxima at $\alpha_1 = 51.72^\circ$ and 54.78° , possibly indicating PPA streaks, which suggests that the coating is not uniform. From optical microscopy images it appears that only $85 \pm 2\%$ of sharkskin is eliminated. After the third load ($t = 26.4 \text{ min}$), the streak formed at $\alpha_1 = 51.72^\circ$ has thickened and become wider, but another, which formed earlier at $\alpha_1 = 54.78^\circ$, has now disappeared or, rather, spread in the lateral direction. Thus, by performing such angular reflectivity sweeps after each extrusion load and translating them into the coating thickness we are able to visualize the PPA coating kinetics (Fig. 9).

The effectiveness of the die coating process may be estimated from the time at which the elimination of sharkskin is complete, which occurs when the die exit is fully coated with fluoropolymer. For the 0.5% PPA/PE blend this occurred after 28 min of extrusion (Figs. 7 and 9), whereas for the 0.1% PPA/PE blend, 10% of sharkskin still remained after 38 min of extrusion (Figs. 6 and 10). Runs with the 0.1% PPA/PE blend were terminated before the steady state developed, but, as seen from Fig. 10, after 40 min of extrusion, the rates of pressure reduction and coating buildup [evaluated at a certain point at the die wall ($\alpha_1 = 52.77^\circ$)] are much lower, as anticipated. The coating thickness achieved was also smaller by a factor of 3. Even though the 0.5% PPA/PE extrudate becomes fracture free after 28 min, approximately 12 more min is needed for both the pressure and the coating thickness to reach steady state ($17.5 \pm 0.2 \text{ MPa}$ and $400 \pm 110 \text{ nm}$, respectively) (Figs. 7 and 9). Here, \pm represents the fluctuating nature of the values in equilibrium. At this time the sapphire die was examined using optical microscopy with a $20\times$ objective, and a characteristic width of $5 \pm 2 \text{ } \mu\text{m}$ of PPA streaks was found (Fig. 9, inset), agreeing well with earlier measurements [Migler *et al.* (2001a)]. By studying the

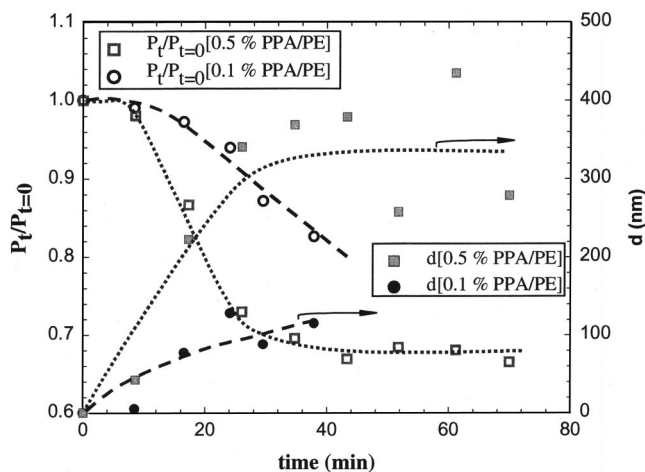


FIG. 10. Effect of the content of PPA in a PPA/PE blend (0.5% blend shown by squares and 0.1% blend shown by circles) on the coating kinetics. Note that the blend pressure (P_t) is normalized by that of pure PE (P_{PE}). Measurements were conducted at $\dot{\gamma} = 112.5 \text{ s}^{-1}$, $T = 180^\circ\text{C}$ and $\alpha_1 = 52.77^\circ$.

coating profile obtained by the frust-TIR approach (Fig. 9), we conclude that the streaks are $7 \pm 2 \mu\text{m}$ wide, which is in reasonable correspondence with the optical microscopy images.

When the apparent shear rate nearly doubled (215 s^{-1}) the steady state coating time using 0.1% PPA/PE is shorter than when the 0.5% PPA/PE blend was run at 112.5 s^{-1} (Figs. 9 and 11). This is consistent with work of Lavallée and Woods (2000) who found a strong decrease in coating time with an increase in throughput. Also, in work of

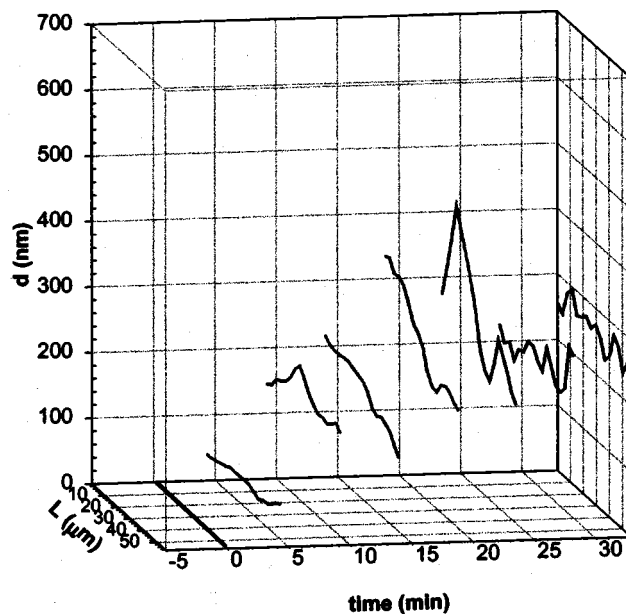


FIG. 11. Visualization of the PPA coating kinetics during extrusion of the (a) 0.1% PPA/PE blend at $\dot{\gamma} = 215 \text{ s}^{-1}$ and $T = 180^\circ\text{C}$.

Rosenbaum *et al.* (1995) it was stated that the coating time should be inversely proportional to the residence time of the fluoropolymer in the die. The steady state coating thickness reached $\approx 70\%$ that developed in the extrusion of 0.5% PPA/PE, and was achieved 15 min earlier. However, just like in case of the 0.5% PPA/PE blend, full sharkskin elimination occurred before the pressure and coating thickness reached steady state (not shown). This observation indicates that, although the die exit may be fully coated (suppressing sharkskin), the final thickness has not been reached, and possibly that bare spots of the coating in the die land are being filled in.

A. Test of minimal coating thickness

In order to understand how thin the coating can be to remain effective in the elimination of sharkskin, pure PE was extruded at an apparent shear rate of 112.5 s^{-1} after the last load (*L8*) of the 0.5% PPA/PE blend was completed (at this time average PPA coating thickness 2 ± 0.1 mm upstream of the die exit reached 400 ± 110 nm, as follows from Fig. 9). Analogous to the coating build-up experiments, angular sweeps were performed at the end of each extrusion load [Fig. 8(b)]. The initial load of the pure PE depleted the fluoropolymer coating quite significantly [Figs. 8(b) and 9], while the reduced pressure was maintained at the level of 17.5 ± 0.2 MPa. After 53 min of continuous PE extrusion (or seven PE loads), the coating thinned to 60 ± 15 nm, but the extrudate surface remained entirely free of any fracture (here \pm represents circumferential variation in coating thickness). This suggested that, even though the PPA thickness was greatly diminished from its steady state value, it was still sufficient to induce slippage at the PPA/PE interface.

In order to construct a model for the coating process, we consider the rate of PPA depletion based on the polymer melt rheology (Fig. 1) and correlate it with the data obtained using frust-TIR measurements (Fig. 9). Because the coating thickness d is on the order of only a few hundred nanometers, we assume a linear velocity profile in the fluoropolymer layer with a stick boundary condition, $v_{\text{PPA}} = \dot{\gamma}_{\text{PPA}} r'$, where r' is the distance from the wall. Then the depleted coating d can be calculated as

$$d = \frac{(l-2)}{\dot{\gamma}_{\text{PPA}} t}, \quad (8)$$

where t is the time required for a given d to migrate from the die entrance to the die exit. Note that because our reflectivity measurements are conducted 2 ± 0.1 mm upstream of the die exit, the PPA must migrate distance $l-2$ mm. Since the experiment for coating depletion is conducted via extrusion of the pure PE, obtaining the shear rate within the PPA layer ($\dot{\gamma}_{\text{PPA}}$) from the capillary rheometry alone is not possible (unless data on pure PPA extrusion are available). Instead, we use oscillatory shear data for pure PPA tested in the ARES rheometer. First, from the steady state pressure that developed during extrusion of the 0.5% PPA/PE blend we calculate the stress $\sigma = PR/(2l) = \eta \dot{\gamma}$, and because at the PPA/PE interface the stress is the same for either PPA or PE, we use it to get the corresponding viscosity and oscillatory frequency (or shear rate) of the PPA from our rheology data (Fig. 1). This allows rewriting Eq. (8) as follows:

$$d = \frac{2\eta_{\text{PPA}} l(l-2)}{PRt}, \quad (9)$$

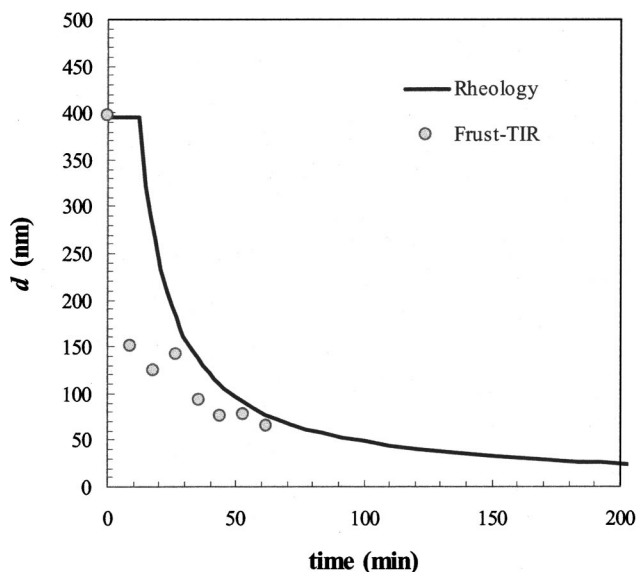


FIG. 12. Kinetics of PPA coating desorption. Measurements were conducted at $\dot{\gamma} = 112.5 \text{ s}^{-1}$ and $T = 180 \text{ }^\circ\text{C}$.

where $\eta_{\text{PPA}} = 1474 \text{ Pa s}$ is the dynamic viscosity of pure PPA obtained from capillary steady state pressure of $P = 17.5 \text{ MPa}$ (Fig. 7) for which the wall shear stress is calculated to be 0.184 MPa . Now, we can estimate the kinetics of coating depletion by plotting d vs t (Fig. 12).

Our frustr-TIR measurements of the coating depletion begin with extrusion of the pure PE at $t = 0 \text{ min}$ which corresponds to the coating thickness of 400 nm that was developed after extrusion of the $L8$ load of the 0.5% PPA/PE blend. According to our model we assume that the coating is uniform along the length of the die. Therefore, from Eq. (9) it is expected that it would take 12.2 min for this coating to migrate from the die entrance to the die exit, as shown in Fig. 12, and we expect this to be an induction time during which the thickness does not change. We find that the initial depletion rate based on the frustr-TIR measurements is faster than our model predicts but as time progresses and the coatings become significantly thinner, both the experimental data and the model predictions appear to be in good agreement. Returning to our assumption of a single fluoropolymer layer, the long time data are consistent with the idea that there is a single layer of fluoropolymer between the wall and the polyethylene, but the short time data may indicate that above this layer the structure is more complex.

B. Elucidation of the coating mechanism

There are indications in the data that the coating occurs upstream of the die exit and that the fluoropolymer migrates downstream along the wall under the influence of shear flow. In particular, we find the correlations between the signals whereby pressure decrease is observed first (which indicates development of a coating somewhere upstream of the die exit) followed by optical observation of the coating 2 mm upstream of the exit, and then the disappearance of sharkskin (indicating coating at the exit). Further, the streak-like nature of the coating seen by microscopy (Fig. 9) suggests formation of the coating upstream followed by downstream migration.

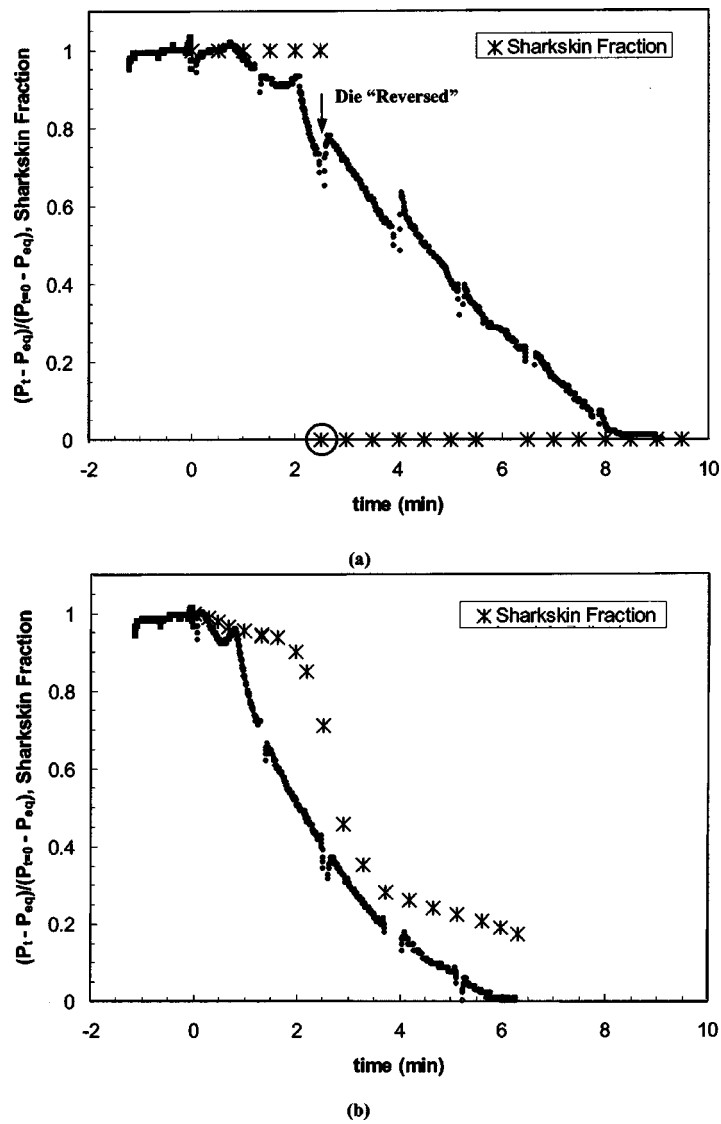


FIG. 13. Elucidation of the coating mechanism via experiments with (a) the die “reversed” at the time indicated by the arrow and (b) the die not reversed. Measurements were conducted with the 0.1% PPA/PE blend at $\dot{\gamma} = 225 \text{ s}^{-1}$ and $T = 180 \text{ }^\circ\text{C}$.

To test this hypothesis, we first extrude pure PE followed by the 0.1% PPA/PE blend for a finite period of time. The die is then “reversed” (turned upside down) in the rheometer and flow is recommenced. This reversal is done at a time when there has been a reduction in pressure (some coating has occurred), but there is still 100% sharkskin in the extrudate. If the fluoropolymer first coats the die at the entrance region, then when the die is reversed, a coating would be present at the exit. Since sharkskin disappearance only occurs when the fluoropolymer is at the exit, this test can detect whether the coating first occurs at the entrance. These experiments are carried out using a steel slit die ($1 \times 8 \times 20$ mm) with a 180° entrance.

In Fig. 13 we plot the reduced pressure values for each load of the blend (P_t) nor-

malized by the steady state values ($P_{\text{eq}} = 10.54 \text{ MPa}$) obtained when the PPA coating was fully developed, and by the pressure of pure PE ($P_{t=0} = 14.01 \text{ MPa}$) at apparent shear rate of 225 s^{-1} and temperature of 180°C . The subsequent sharkskin fraction was plotted along with the normalized pressure versus the extrusion time. Figure 13(a) shows that during extrusion of the 0.1% PPA/PE blend, the die was reversed when the pressure dropped by about 7.2% [or when $(P_t - P_{\text{eq}}/P_{t=0} - P_{\text{eq}}) = 0.73$]. As extrusion was recommenced after reversal, the sharkskin disappeared *instantaneously* and *completely*, while the reduced pressure remained unchanged. This shows that in the time just before flow had stopped, the fluoropolymer had fully coated the die entrance, but the die exit contained no fluoropolymer. The result was reproduced in repeated experiments. After this experiment was completed, the die and extruder barrel were cleaned, and we ran the experiment in “normal” mode i.e., without reversing the die. If the hypothesis that coating starts forming at the die entrance were true, then the time for full sharkskin elimination in this experiment would be significantly longer, and the character of the elimination would be gradual, rather than abrupt. Indeed, the sharkskin disappeared slowly, even though the pressure was reduced significantly [Fig. 13(b)]. Then the coating process accelerated, after which it slowed down again, with $19 \pm 2\%$ of sharkskin still remaining after 6 min of extrusion, as seen from Fig. 13(b).

Since it was found that the PPA coating first occurs at the die entrance, we decided to estimate the migration speed of the PPA droplets along the die walls. An experiment was performed in which a clean sapphire die was locally precoated by solution casting only at its entrance. Approximately 12% of the die length ($l/D = 33.4/1.6$) was dipped into a solution of the fluoropolymer in acetone, which produced a $7 \mu\text{m}$ thick coating (on average) as measured by the change in mass. When PE was extruded through such a die at temperature of 180°C and apparent shear rate of 225 s^{-1} (not shown), the pressure was reduced to 80% of its initial value in 1.35 min, while the sharkskin persisted for 58.6 s of extrusion. After that the first smooth streak appeared, and 23 s later the instability vanished. This experiment demonstrated that the PPA migrated along the die wall at an estimated migration speed of the PPA front of approximately $0.45 \pm 0.05 \text{ mm/s}$. As the experiment with the entrance precoated die was run further, the pressure kept rising while the extrudate still remained free of any fracture, suggesting that the fluoropolymer coating that had been initially applied at the die entrance was being removed, and that the bare area was spreading toward the die exit. Finally, when the pressure reached 89% of its initial value (at $t = 35 \text{ min}$), the first sharkskin streak reappeared, thereby identifying coating depletion from the die exit. In the case of extrusion of the PE in which only the die exit was precoated with the PPA, the pressure reduced by only 6% while the sharkskin was eliminated instantaneously. It then took 40 min for the first sharkskin streak to reappear.

Based on the die-reversal and localized precoating experiments, we suggest that during blend extrusion, the PPA droplets first adsorb at the die entrance (which explains the reduction in pressure), possibly due to strong recirculating flow in the 180° -entrance geometry as suggested by [Kanu and Shaw (1982)], and then they migrate toward the die exit under the influence of the shear field. Note that while our results point out the importance of the entrance region, they do not rule out the possibility of subsequent adsorption along the die wall.

C. Model for the steady state coating thickness

Using the technique of frust-TIR we can obtain experimental data for the kinetics of the fluoroelastomer coating process, estimate the steady state coating thickness at the exit as well as the minimal coatings for the polymer–polymer slippage *in situ*. With this

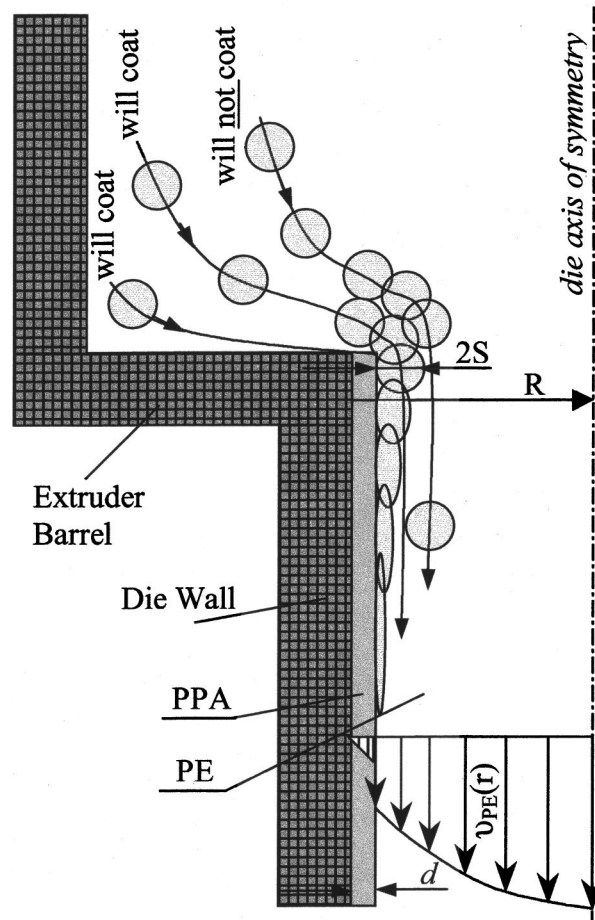


FIG. 14. Schematic of PPA/PE flow in a circular die.

information, we are motivated to develop a simple model that predicts steady state coating thickness d at the exit and the coating kinetics. The model is based on the balance between the mass flow rate of the fluoroelastomer that coats the die (Q_{in}) and the mass flow rate of the fluoroelastomer leaving the die due to convection downstream (Q_{out}).

From the die-reversal experiment we learned that the coating process starts with preferential adsorption of the PPA droplets at the die entrance. In our model, we assume no cross streamline droplet migration. We assume that a droplet (of radius S) will coat the wall if its streamline is within a distance S from the wall, otherwise it will not coat it. This is schematically shown in Fig. 14 where upon contact with the wall, the PPA droplet sticks and spreads downstream, thereby coating the wall. Our model does not consider any additional mechanism for deposition of the PPA material.

It was shown in Sec. III A that depletion of the PPA coating occurred due to convection of the fluoropolymer downstream of the die. Thus the mass flow rate of the coating material leaving the die is based upon a linear velocity profile of the fluoropolymer layer. This allows us to write the equations for the mass flow rates of the fluoropolymer in and out of the die as

$$Q_{\text{in}} = \int_0^{2\pi} \int_0^S C[v_{\text{PE}}(r')]Rdr'd\varphi = 2RSC\pi\left(\frac{\dot{\gamma}_{\text{PE}}S}{2} + V_S\right), \quad (10)$$

$$Q_{\text{out}} = \int_0^{2\pi} \int_0^d \rho v_{\text{PPA}}(r')dr'Rd\varphi = R\rho\dot{\gamma}_{\text{PPA}}d^2\pi, \quad (11)$$

where r' is the distance from the wall, R is the die radius, C is the bulk concentration of the PPA in the PPA/PE blend, ρ is the density of the PPA, and $v_{\text{PE}}(r')$ is the velocity of the polyethylene near the wall given by $v_{\text{PE}}(r') = \dot{\gamma}_{\text{PE}}(R,t)r' + V_S(\dot{\gamma},t)$. The slippage at the PE/PPA interface is taken into account by the slippage velocity $V_S(\dot{\gamma},t)$. V_S is a function of t because at the beginning of the process, the PE is in direct contact with the wall and we expect little/no slippage, whereas in the steady state when the wall is fully coated, we anticipate strong slippage. In the steady state we equate the right-hand sides of Eqs. (10) and (11) as

$$2CS\left(\frac{\dot{\gamma}_{\text{PE}}S}{2} + V_S\right) = \rho\dot{\gamma}_{\text{PPA}}d^2. \quad (12)$$

At the beginning of the process, $(\dot{\gamma}_{\text{PE}}S/2)$ is an important factor for the coating kinetics. However, as the system reaches steady state and the die walls become fully coated, V_S dominates the sum of Eq. (12) and d can be expressed as

$$d = \left(\frac{2CV_S S}{\rho\dot{\gamma}_{\text{PPA}}}\right)^{0.5}. \quad (13)$$

All the parameters in Eq. (13) were presented earlier with the exception of V_S . To estimate V_S we use data by Migler *et al.* (2001b) who utilized the same class of materials (but with different molecular properties), and found that over the current range of shear rates, the slippage velocity scaled nearly linearly with the apparent shear rate: $V_S = (0.1 \text{ mm})\dot{\gamma}$. With these values, we obtain a predicted steady state coating of $d = 690 \text{ nm}$ compared to the measured value of $400 \pm 110 \text{ nm}$ (Fig. 9). For the 0.1% PPA/PE blend extruded at higher shear rate ($\dot{\gamma} = 215 \text{ s}^{-1}$) the model predicts a steady state coating of 310 nm , which is very close to the measured value of $250 \pm 50 \text{ nm}$ (Fig. 11). An important observation which can be drawn from Eq. (13) is that the steady state coating thickness at the exit appears to be independent of the die diameter and scales with the droplet size, which is consistent with the recent work by Oriani and Chapman (2003).

IV. CONCLUSION

Using a newly developed technique based on frust-TIR, die-reversal and localized pre-coating experiments, we conclude that during the extrusion of PPA/PE blends the PPA droplets first adsorb at the die entrance, and then migrate toward the die exit, and apparent form streaks. At the PPA/PE interface of these streaks, the velocity gradient and the wall shear stress are reduced. The question of whether the droplets also adsorb along the die wall further downstream remains.

Monitoring the streak kinetics suggests that they are circumferentially nonuniform, which may be explained by the wide distribution in PPA droplet size and their dispersion characteristics in the PE matrix. Despite the steady state coating thickness reached, $\approx 400 \text{ nm}$, the *necessary* coating thickness for the PPA layer is found to be less than 60 nm . Both the steady state and the *minimal* coatings are thinner than the $5\text{--}15 \mu\text{m}$ reported in earlier work, where the coating thickness was evaluated by secondary ion mass

spectrometric and scanning electron microscopic analyses [Lo *et al.* (1999)]. Thickness comparable to the radius of gyration of the fluoroelastomer appears to be sufficient to induce interfacial slippage as long as the die exit is coated *uniformly*. This is consistent with the results of Migler *et al.* (1993) who showed that a short-chain monolayer was sufficient to alter a polymer–wall interface and allow polymer–wall slippage.

Our measurements described the fluoropolymer coating kinetics during the extrusion of PPA/PE blends at constant temperature and for dies with 180°-entrance geometry. The mass flow rate balance model shows that important parameters that determine the magnitude of the steady state coating thickness were the concentration of the PPA and the size of the PPA droplets. However, the role of such parameters as the relative elasticity of PPA and the mainstream polymer, their molecular weight distribution and the normal stress effects as well as the effect of flow streamlines that develop at the die entrance appear to be inherently important in controlling the coating kinetics as well.

ACKNOWLEDGMENTS

The authors wish to thank S. Oriani, C. Macosko, H. Stone, D. Bigio, M. Meillon, D. Morgan, and S. Roth for useful advice and critical discussions. They thank the reviewers for insightful comments. Certain equipment, instruments or materials are identified in this paper in order to adequately specify experimental details. Such identification does not imply recommendation by the National Institute of Standards and Technology nor does it imply the materials are necessarily the best available for the purpose.

References

- Achilleos, E. C., G. Georgiou, and S. G. Hatzikiriakos, "Role of processing aids in the extrusion of molten polymers," *J. Vinyl Addit. Technol.* **8**, 7–24 (2002).
- Amos, S. E., G. M. Giacomello, J. H. Horns, C. Lavallée, and S. S. Woods, "Polymer processing aids (PPA)," *Plastic Additives* (Hanser, Munich, 2001).
- Barone, J. R., and S. Q. Wang, "Rheo-optical observations of sharkskin formation in slit-die extrusion," *J. Rheol.* **45**, 1–12 (2001).
- Beaufils, P., B. Vergnes, and J. F. Agassant, "Characterization of the sharkskin defect and its development with the flow conditions," *Int. Polym. Process.* **4**, 78–84 (1989).
- Bergem, N., "Visualization studies of polymer melt flow anomalies in extrusion," VIIIth International Congress of Rheology, 1976, pp. 50–54.
- Born, W., and E. Wolf, *Principles of Optics* (Pergamon, Oxford, 1993).
- Brochard-Wyart, F., "Slippage at the interface between two slightly incompatible polymers," *C. R. Acad. Sci., Ser. II: Mec., Phys., Chim., Sci. Terre Univers* **310**, 1169–1173 (1990).
- Brochard-Wyart, F., and P. G. de Gennes, "Sliding molecules at a polymer-polymer interface," *C. R. Acad. Sci., Ser. II: Mec., Phys., Chim., Sci. Terre Univers* **317**, 13–17 (1993).
- Brochard-Wyart, F., P. G. de Gennes, and P. Pincus, "Suppression of sliding at the interface between incompatible polymer melts," *C. R. Acad. Sci., Ser. II: Mec., Phys., Chim., Sci. Terre Univers* **314**, 873–878 (1992).
- Chan, P. C. H., and L. G. Leal, "Motion of a deformable drop in a 2nd-order fluid," *J. Fluid Mech.* **92**, 131–170 (1979).
- Cogswell, F. N., "Stretching flow instabilities at the exits of extrusion dies," *J. Non-Newtonian Fluid Mech.* **2**, 37–47 (1977).
- Coulliette, C., and C. Pozrikidis, "Motion of an array of drops through a cylindrical tube," *J. Fluid Mech.* **358**, 1–28 (1998).
- Court, I. N., and F. K. von Willisen, "Frustrated total internal reflection and application of its principle to laser cavity design," *Appl. Opt.* **3**, 719–726 (1964).
- Dao, T. T., and L. A. Archer, "Relaxation dynamics of entangled polymer liquids near solid substrates," *Langmuir* **17**, 4042–4049 (2001).
- de Fornel, F., *Evanescent Waves* (Springer, Berlin, 2001).
- Denn, M. M., "Extrusion instabilities and wall slip," *Annu. Rev. Fluid Mech.* **33**, 265–287 (2001).

- Dhori, P. K., R. S. Jeyaseelan, A. J. Giacomini, and J. C. Slattery, "Common line motion. 3. Implications in polymer extrusion," *J. Non-Newtonian Fluid Mech.* **71**, 231–243 (1997).
- Eichenwald, A., "On the energy motion on total internal reflection of light," *J. Russ. Phys.-Chem. Soc.* **41**, 131 (1909).
- El Kissi, N., and J. M. Piau, "Adhesion of linear low-density polyethylene for flow regimes with sharkskin," *J. Rheol.* **38**, 1447–1463 (1994).
- Everage, A. E., "Theory of stratified bicomponent flow of polymer melts. I. Equilibrium Newtonian tube flow," *Trans. Soc. Rheol.* **17**, 629–646 (1973).
- Ferry, J. D., *Viscoelastic Properties of Polymers* (Wiley, New York, 1980).
- Ghanta, V. G., B. L. Riise, and M. M. Denn, "Disappearance of extrusion instabilities in brass capillary dies," *J. Rheol.* **43**, 435–442 (1999).
- Goveas, J. L., and G. H. Fredrickson, "Apparent slip at a polymer-polymer interface," *Eur. Phys. J. B* **2**, 79–92 (1998).
- Graham, M. D., "The sharkskin instability of polymer melt flows," *Chaos* **9**, 154–163 (1999).
- Hall, E. E., "The penetration of totally reflected light into the rarer medium," *Phys. Rev.* **15**, 73 (1902).
- Harrick, N. J., *Internal Reflection Spectroscopy* (Interscience, New York, 1967).
- Hatzikiriakos, S. G., and J. M. Dealy, "Effects of interfacial conditions on wall slip and sharkskin melt fracture of HDPE," *Int. Polym. Process.* **8**, 36–44 (1993).
- Hatzikiriakos, S. G., P. Hong, W. Ho, and C. W. Stewart, "The effect of Teflon™ coatings in polyethylene capillary extrusion," *J. Appl. Polym. Sci.* **55**, 595–603 (1995).
- Hong, Y., J. J. Cooper-White, M. E. Mackay, C. J. Hawker, E. Malmström, and N. Rehnberg, "A novel processing aid for polymer extrusion: Rheology and processing of polyethylene and hyperbranched polymer blends," *J. Rheol.* **43**, 781–793 (1999).
- Hong, Y., S. J. Coombs, J. J. Cooper-White, M. E. Mackay, C. J. Hawker, E. Malmström, and N. Rehnberg, "Film blowing of linear low-density polyethylene blended with a novel hyperbranched polymer processing aid," *Polymer* **41**, 7705–7713 (2000).
- Howells, E. R., and J. Benbow, "Flow defects in polymer melts," *Trans. J. Plastics Inst.* **30**, 240–253 (1962).
- Inn, Y. W., R. J. Fischer, and M. T. Shaw, "Visual observation of development of sharkskin melt fracture in polybutadiene extrusion," *Rheol. Acta* **37**, 573–582 (1998).
- Inn, Y. W., L. S. Wang, and M. T. Shaw, "Efforts to find stick-slip flow in the land of a die under sharkskin melt fracture conditions: Polybutadiene," *Macromol. Symp.* **158**, 65–75 (2000).
- Joseph, D. D., K. Nguyen, and G. S. Beavers, "Non-uniqueness and stability of the configuration of flow of immiscible fluids with different viscosities," *J. Fluid Mech.* **141**, 319–345 (1984).
- Kalika, D. S., and M. M. Denn, "Wall slip and extrudate distortion in linear low-density polyethylene," *J. Rheol.* **31**, 815–834 (1987).
- Kanu, R. C., and M. T. Shaw, "Rheology of polymer blends—Simultaneous slippage and entrance pressure loss in the ethylene-propylene-diene (Epdm) Viton system," *Polym. Eng. Sci.* **22**, 507–511 (1982).
- Kim, S., and J. M. Dealy, "Gross melt fracture of polyethylene. I: A criterion based on tensile stress," *Polym. Eng. Sci.* **42**, 482–494 (2002a).
- Kim, S., and J. M. Dealy, "Gross melt fracture of polyethylene. II: Effects of molecular structure," *Polym. Eng. Sci.* **42**, 495–503 (2002b).
- Kok, P. J. A. H., S. G. Kazarian, C. J. Lawrence, and B. J. Briscoe, "Near-wall particle depletion in a flowing colloidal suspension," *J. Rheol.* **46**, 481–493 (2002).
- Lam, Y. C., L. Jiang, C. Y. Yue, K. C. Tam, and L. Li, "Interfacial slip between polymer melts studied by confocal microscopy and rheological measurements," *J. Rheol.* **47**, 795–807 (2003).
- Larson, R. G., "Instabilities in viscoelastic flows," *Rheol. Acta* **31**, 213–263 (1992).
- Lavallée, C., and S. S. Woods, "Die geometry and polymer processing additive (Ppa) efficiency," *SPE ANTEC Tech. Papers* **58**, 2857–2861 (2000).
- Li, X. F., and C. Pozrikidis, "Wall-bounded shear flow and channel flow of suspensions of liquid drops," *Int. J. Multiphase Flow* **26**, 1247–1279 (2000).
- Lo, H. H. K., C. M. Chan, and S. H. Zhu, "Characterization of the lubricant layer formed at the interface between the extrudate and the die wall during the extrusion of high density polyethylene and fluoroelastomer blends by XPS, SIMS and SEM," *Polym. Eng. Sci.* **39**, 721–732 (1999).
- Lyngaae-Jorgensen, J., "On the influence of interfacial slip on melt flow properties of polymer blends," *Int. Polym. Process.* **2**, 123–130 (1988).
- Mackley, M. R., R. P. G. Rutgers, and D. G. Gilbert, "Surface instabilities during the extrusion of linear low density polyethylene," *J. Non-Newtonian Fluid Mech.* **76**, 281–297 (1998).
- McCrackin, F. L., E. Passaglia, R. R. Stromberg, and H. L. Steinberg, "Measurement of the thickness and refractive index of very thin films and the optical properties of surfaces by ellipsometry," *J. Res. Natl. Inst. Stand. Technol.* **106**, 589–603 (2001).
- Migler, K. B., H. Hervet, and L. Leger, "Slip transition of a polymer melt under shear stress," *Phys. Rev. Lett.* **70**, 287–290 (1993).

- Migler, K. B., Y. Son, F. Qiao, and K. Flynn, "Extensional deformation, cohesive failure, and boundary conditions during sharkskin melt fracture," *J. Rheol.* **46**, 383–400 (2002).
- Migler, K. B., C. Lavallée, M. P. Dillon, S. S. Woods, and C. L. Gettinger, "Flow visualization of polymer processing additives effects," *SPE ANTEC Tech. Papers* **1**, 1132–1136 (2001a).
- Migler, K. B., C. Lavallée, M. P. Dillon, S. S. Woods, and C. L. Gettinger, "Visualizing the elimination of sharkskin through fluoropolymer additives: Coating and polymer–polymer slippage," *J. Rheol.* **45**, 565–581 (2001b).
- Mortazavi, S., and G. Tryggvason, "A numerical study of the motion of drops in Poiseuille flow. Part 1. Lateral migration of one drop," *J. Fluid Mech.* **411**, 325–350 (2000).
- Moynihan, R. H., D. G. Baird, and R. Ramanathan, "Additional observations on the surface melt fracture behavior of linear low-density polyethylene," *J. Non-Newtonian Fluid Mech.* **36**, 255–263 (1990).
- Newton, I., *Optics: or, A Treatise of the Reflections, Refractions, Inflections and Colours of Light; based on the 4th edition, London, 1730* (Dover, New York, 1979).
- Oliver, D. R., "Influence of particle rotation on radial migration in the Poiseuille flow of suspensions," *Nature (London)* **194**, 1269–1271 (1962).
- Oriani, S. R., and G. R. Chapman, "Fundamentals of melt fracture elimination using fluoropolymer process aids," *SPE ANTEC Tech. Papers* **49**, 22–26 (2003).
- Park, C. C., F. Baldessari, and L. G. Leal, "Study of molecular weight effects on coalescence: Interface slip layer," *J. Rheol.* **47**, 911–942 (2003).
- Parsons, D., R. Harrop, and E. G. Mahers, "The kinetics of particle and polymer adsorption by total internal-reflection fluorescence," *Colloids Surf.* **64**, 151–160 (1992).
- Person, T. J., and M. M. Denn, "The effect of die materials and pressure-dependent slip on the extrusion of linear low-density polyethylene," *J. Rheol.* **41**, 249–265 (1997).
- Petrie, C. J. S., and M. M. Denn, "Instabilities in polymer processing," *AIChE J.* **22**, 209–236 (1976).
- Piau, J.-M., and J. F. Agassant, *Rheology for Polymer Melt Processing* (Elsevier Science, Amsterdam, 1996).
- Piau, J. M., N. El Kissi, and B. Tremblay, "Low Reynolds-number flow visualization of linear and branched silicones upstream of orifice dies," *J. Non-Newtonian Fluid Mech.* **30**, 197–232 (1988).
- Piau, J. M., N. El Kissi, and B. Tremblay, "Influence of upstream instabilities and wall slip on melt fracture and sharkskin phenomena during silicones extrusion through orifice dies," *J. Non-Newtonian Fluid Mech.* **34**, 145–180 (1990).
- Prieve, D. C., "Measurement of colloidal forces with TIRM," *Adv. Colloid Interface Sci.* **82**, 93–125 (1999).
- Ramamurthy, A. V., "Wall slip in viscous fluids and influence of materials of construction," *J. Rheol.* **30**, 337–357 (1986).
- Rosenbaum, E. E., S. G. Hatzikiriakos, and C. W. Stewart, "Flow implications in the processing of tetrafluoroethylene/hexafluoropropylene copolymers," *Int. Polym. Process.* **10**, 204–212 (1995).
- Shih, C. K., "Rheological properties of incompatible blends of 2 elastomers," *Polym. Eng. Sci.* **16**, 742–746 (1976).
- Shizgal, B., H. L. Goldsmith, and S. G. Mason, "The flow of suspensions through tubes IV: Oscillatory flow of rigid spheres," *Can. J. Chem. Eng.* **43**, 97–101 (1965).
- Vinogradov, G. V., "Viscoelasticity of polymeric systems in fluid and rubbery states in uniaxial extension and shear," *Pure Appl. Chem.* **42**, 527–549 (1975).
- Wang, S. Q., P. A. Drda, and Y. W. Inn, "Exploring molecular origins of sharkskin, partial slip, and slope change in flow curves of linear low density polyethylene," *J. Rheol.* **40**, 875–898 (1996).
- Wise, G. M., M. M. Denn, and A. T. Bell, "Near-surface dynamics of sheared polymer melts using ATR/FTIR," *AIChE J.* **44**, 701–710 (1998).
- Wise, G. M., M. M. Denn, A. T. Bell, J. W. Mays, K. Hong, and H. Iatrou, "Surface mobility and slip of polybutadiene melts in shear flow," *J. Rheol.* **44**, 549–567 (2000).
- Wood-Adams, P. M., J. M. Dealy, A. W. de Groot, and O. D. Redwine, "Effect of molecular structure on the linear viscoelastic behavior of polyethylene," *Macromolecules* **33**, 7489–7499 (2000).
- Xing, K. C., and H. P. Schreiber, "Fluoropolymers and their effect on processing linear low-density polyethylene," *Polym. Eng. Sci.* **36**, 387–393 (1996).
- Zhao, R., and C. W. Macosko, "Slip at polymer-polymer interfaces: Rheological measurements on coextruded multilayers," *J. Rheol.* **46**, 145–167 (2002).
- Zhou, H., and C. Pozrikidis, "Pressure-driven flow of suspensions of liquid drops," *Phys. Fluids* **6**, 80–94 (1994).